ChemPubSoc Europe

DOI: 10.1002/cssc.201601683

CHEMSUSCHEM Full Papers

Tetraphenylmethane-Arylamine Hole-Transporting Materials for Perovskite Solar Cells

Xuepeng Liu,[a, b] Fantai Kong,*[a] Tai Cheng,[c] Wangchao Chen,[a, b] Zhan'ao Tan,*[c] Ting Yu,[a, b] Fuling Guo,[a] Jian Chen,[a] Jianxi Yao,[c] and Songyuan Dai*[a, c]

A new class of hole-transporting materials (HTM) containing tetraphenylmethane (TPM) core have been developed. After thermal, charge carrier mobility, and contact angle tests, it was found that TPA-TPM (TPA: arylamine derivates side group) showed higher glass-transition temperature and larger water-contact angle than spiro-OMeTAD with comparable hole mobility. Photoluminescence and impedance spectroscopy studies indicate that TPA-TPM's hole-extraction ability is comparable to that of spiro-OMeTAD. SEM and AFM results suggest that TPA-TPM has a smooth surface. When TPA-TPM is used in mesoscopic perovskite solar cells, power conversion efficiency comparable to that of spiro-OMeTAD is achieved. Notably, the perovskite solar cells employing TPA-TPM show better long-term stability than that of spiro-OMeTAD. Moreover, TPA-TPM can be prepared from relatively inexpensive raw materials with a facile synthetic route. The results demonstrate that TPM-arylamines are a new class of HTMs for efficient and stable perovskite solar cells.

Introduction

Organic–inorganic metal halide perovskites (ABX_3, $A = CH_3NH_3$ or $NHCHNH_3$, B = Pb, X = Br, I, or Cl) have drawn great attention as excellent light-harvesting materials because of their direct band gap, large exciton-diffusion lengths, and excellent ambipolar mobility.[1–4] Power conversion efficiency (PCE) of perovskite solar cells (PSCs) exceeding 20%[5,6] has been achieved. In PSCs, hole-transporting materials (HTMs) play an important role in collecting and transferring hole, and enhancing the stability of the devices.[7,8] To date, spiro-OMeTAD (2,2′,7,7′-Tetrakis-(N,N-di-4-methoxyphenylamino)-9,9′-spirobifluorene) is the most commonly HTM used in high-efficiency devices. However, the multistep low-yield synthesis and difficult purification process of spiro-OMeTAD limit its practical applications.[9] Moreover, the stability of PSCs based on spiro-OMeTAD is relatively poor. Therefore, to reduce the cost of cell fabrication, lots of molecular organic HTMs have been developed for PSCs. Among the reported HTMs, star-shaped molecules have proved to be efficient HTMs in PSCs. They are usually obtained by varying the cores and connecting arylamine derivatives. At present, the triptycene,[10] thiophene,[11,12] triphenylamine,[13] benzene,[14,15] triazine,[16] bifluorenylidene,[17] [2.2]paracyclophane,[18] indolocarbazole,[19] tetraarylethene,[20] carbazole,[9] benzotrithiophene,[21] azulene,[22] truxene,[23,24] cores or their derivatives and some new spiral cores[25–29] have been reported. However, some of those reported HTMs suffer relatively poor stability or lower PCE than spiro-OMeTAD. On the other hand, to reduce the costs of HTM in PSCs, new inexpensive HTMs with facile synthetic routes need to be developed.

Previously, non-twist and star-burst tetraphenylmethane (TPM) unit were reported with high thermal stability and good contact with different layers in organic light-emitting diodes (OLEDs), organic solar cells, or single-molecule junction devices with gold electrodes.[30–34] In addition, TPM can be prepared from relatively low-cost raw materials with a facile synthetic route (illustrated in the Experimental Section and Supporting Information). To elucidate the advantage of the TPM unit, we try to introduce TPM as the core to develop new, stable, and efficient HTMs. Two new compounds (DPA-TPM and TPA-TPM) with TPM as core and bulky arylamine side groups (DPA or TPA) as terminal groups and a reference compound with anisole as terminal group (Ph-TPM) were synthesized, as shown in Figure 1. Among these new compounds, TPA-TPM shows good solubility in common organic solvents, high thermal stability, good film-forming ability, large water-contact angle, high hole mobility, and suitable HOMO level compared to $CH_3NH_3PbI_3$. Owing to these advantages of TPA-TPM, the PSCs built with it show comparable PCE and better long-term stability than that of spiro-OMeTAD. The easy synthesis of TPA-TPM and high PCE of the device enable us to prepare other inexpensive and efficient HTMs incorporating TPM core.

[a] Dr. X. Liu, Prof. F. Kong, Dr. W. Chen, Dr. T. Yu, Dr. F. Guo, Prof. J. Chen, Prof. S. Dai
Key Laboratory of Novel Thin-film Solar Cells
Institute of Applied Technology
Hefei Institutes of Physical Science
Chinese Academy of Sciences
Hefei, Anhui, 230088 (P.R. China)
E-mail: kongfantai@163.com

[b] Dr. X. Liu, Dr. W. Chen, Dr. T. Yu
University of Science and Technology of China
Hefei, 230026 (P.R. China)

[c] Dr. T. Cheng, Prof. Z. Tan, Prof. J. Yao, Prof. S. Dai
Beijing Key Laboratory of Novel Thin-Film Solar Cells
North China Electric Power University
Beijing, 102206 (P.R. China)
E-mail: sydai@ncepu.edu.cn

Supporting Information of this article can be found under: http://dx.doi.org/10.1002/cssc.201601683.

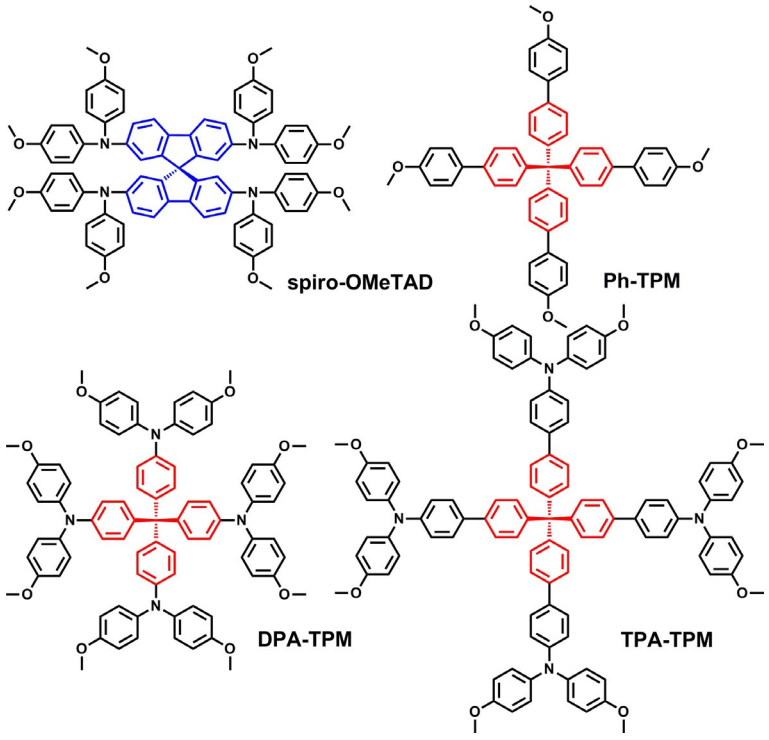

Figure 1. Chemical structures of synthesized HTMs with TPM core and spiro-OMeTAD.

Results and Discussion

The UV/Vis absorption and photoluminescence (PL) properties of the new compounds were investigated, as presented in Figure 2a. DPA-TPM and TPA-TPM show absorption peaks at 308 and 342 nm. The spectrum of TPA-TPM is red-shifted compared to the ones from DPA-TPM and Ph-TPM, which could result from the extension of the π-conjugation by inserting a phenyl ring between the TPM core and diphenylamine arms. The absorption spectrum confirmed that DPA-TPM and TPA-TPM do not compete significantly with $CH_3NH_3PbI_3$ in devices for light harvesting. The PL spectra of DPA-TPM and TPA-TPM show a large Stokes shift of 85 and 103 nm, which indicates that significant changes in geometrical structure of molecules would occur in the excited state.[35] The optical band gaps (E_g) of Ph-TPM, DPA-TPM and TPA-TPM estimated from the intersection of normalized PL and absorption spectra are 4.03, 3.36, and 3.13 eV, respectively.

The electrochemical properties of the investigated compounds was evaluated by cyclic voltammetry (CV) measurements in CH_2Cl_2 solution, as shown in Figure 2b and Figure S2 (in the Supporting Information). The redox peaks of Ph-TPM, DPA-TPM, and TPA-TPM are highly reversible and show good reproducibility, suggesting that they have excellent electrochemical stability.[10] The calculated HOMO levels of Ph-TPM, DPA-TPM, TPA-TPM, and spiro-OMeTAD are −5.36, −5.32, −5.29, and −5.13 eV, respectively. The reported HOMO level of $CH_3NH_3PbI_3$ is around −5.43 eV,[7] which indicates that the compounds reported here should have favorable energetics for hole extraction. LUMO levels of Ph-TPM, DPA-TPM, and TPA-TPM calculated from the CVs and UV/Vis data are −1.33, −1.96, and −2.16 eV. The higher LUMO levels of the new compounds than the conduction band of $CH_3NH_3PbI_3$ can block the electrons from $CH_3NH_3PbI_3$ to the Au counter electrode and ensure carrier transfer at the $CH_3NH_3PbI_3$/HTM interface when the HTMs are excited (see below, Figure 5b).

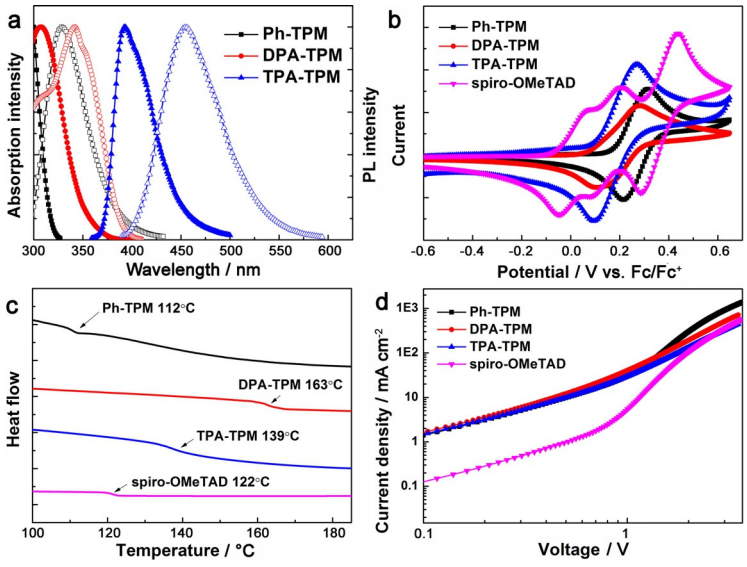

Figure 2. a) UV/Vis absorption and PL spectra in CH_2Cl_2, b) CV with ferrocene as the reference, c) DSC curves, and d) SCLC hole-mobility measurements of spiro-OMeTAD, Ph-TPM, DPA-TPM and TPA-TPM.

The thermal properties of the new compounds were studied by differential scanning calorimetry (DSC) measurements. The glass transition temperature (T_g) of Ph-TPM, DPA-TPM, TPA-TPM, and spiro-OMeTAD are 112, 163, 139 and 122 °C (Figure 2c). The higher T_g of TPA-TPM than that of spiro-OMeTAD demonstrates a more stable amorphous state, which is beneficial to the device stability.[36]

To determine the charge-carrier mobility, hole-only devices (ITO/PEDOT:PSS/HTM/Au; ITO = indium tin oxide, PEDOT:PSS = poly(3,4-ethylenedioxythiophene) polystyrene sulfonate) were fabricated and measured from the space-charge limited current (SCLC) method in the current–voltage (*J–V*) curves (Figure 2d). The thickness of Ph-TPM, DPA-TPM, TPA-TPM, and spiro-OMeTAD is 26, 32, 45, and 40 nm, respectively. The hole mobilities of Ph-TPM, DPA-TPM, TPA-TPM, and spiro-OMeTAD evaluated using the Mott–Gurney law are 8.05×10^{-6}, 3.88×10^{-6}, 1.05×10^{-5} and 1.31×10^{-5} $cm^2V^{-1}s^{-1}$, respectively. Notably, the extension of the π-conjugation by inserting a phenyl ring between the TPM core and diphenylamine arms can improve the hole mobility. The optical, electrochemical, thermal properties, and hole mobility of the new compounds are summarized in Table 1.

To study the hydrophobicity of the new compounds and spiro-OMeTAD, we measured the water-contact angles of these compounds. As shown in Figure S1, Ph-TPM, DPA-TPM, TPA-TPM, and spiro-OMeTAD film show a water-contact angle of around 70, 71, 85, and 72°, respectively. The doped-TPA-TPM and spiro-OMeTAD show a water-contact angle at 84 and 74°, respectively. The shadowed center of Ph-TPM and DPA-TPM in Figure S1 can be a result of their poor films. The higher water-contact angle observed for TPA-TPM in comparison with spiro-OMeTAD may be owed to its superior solubility in chlorobenzene and high aggregation tendency.[30]

The film morphology of these HTMs and spiro-OMeTAD were analyzed by SEM and AFM. Figure 3 shows a top view of the perovskite and perovskite covered by the new compounds and spiro-OMeTAD, and Figure 4 shows AFM topographical images of DPA-TPM, TPA-TPM, and spiro-OMeTAD. The perovskites covered by Ph-TPM and DPA-TPM show a relatively rough surface. The root-mean-square (RMS) roughness of films DPA-TPM, TPA-TPM, and spiro-OMeTAD is 11.9, 1.2, and 2.13 nm, respectively. TPA-TPM shows a slightly smoother surface than that of spiro-OMeTAD, which can also explain why TPA-TPM films have a large water-contact angle. Moreover, the extension of the π-conjugation by inserting a phenyl ring between the TPM core and diphenylamine arms can improve the film-forming ability.

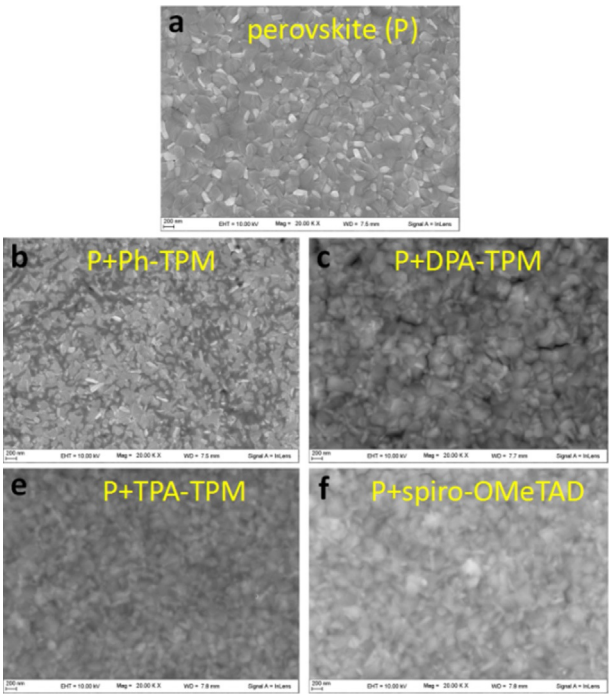

Figure 3. SEM images (top view) of the perovskite layers covered by the new compounds and spiro-OMeTAD.

To investigate the performance of the new compounds as HTMs in PSCs, the mesoscopic PSCs were fabricated and a schematic architecture of the devices is shown in Figure 5a. Figure 5b shows the energy level diagram of each component in the PSCs.

As the PSCs were reported to exhibit a striking enhancement in devices' performance when increasing the conductivity of HTMs by doping 4-*tert*-butylpyridine (*t*BP) and lithium bis(trifluoromethanesulfonyl)imide (LiTFSI) into the HTM,[37] we fabricated the device by doping *t*BP and LiTFSI into all HTM layers. The detailed fabrication of PSCs is shown in the Experimental Section.

The photovoltaic performances of the devices employing the new compounds and spiro-OMeTAD as HTMs were measured under AM 1.5G illuminations (100 $mW\,cm^{-2}$). Figure 6a shows the *J–V* curves obtained for the cells using these HTMs, as summarized in Table 2. The PCEs of PSC devices with Ph-TPM and DPA-TPM are only 4.62 and 9.33%, respectively. The poor performance of these devices with Ph-TPM and DPA-TPM can be a result of their inferior hole mobility and bad film-forming ability, which could be observed from SEM images and high standard deviation from the parameter values of the devices based on them (shown in the Supporting Information).

When the HTM layer is replaced by the soluble TPA-TPM, the performance of the PSC device shows significant improvement, and yields a short-circuit

Table 1. Optical, electrochemical, thermal properties, and hole mobility of Ph-TPM, DPA-TPM, and TA-TPM.

Molecule	λ_{abs} [nm]	E_g[a] [eV]	HOMO[b] level [eV]	LUMO[c] level [eV]	T_g [°C]	*M* [$cm^2V^{-1}s^{-1}$][d]
Ph-TPM	–	4.03	−5.36	−1.33	112	8.05×10^{-6}
DPA-TPM	308	3.36	−5.32	−1.96	163	3.88×10^{-6}
TPA-TPM	342	3.13	−5.29	−2.16	139	1.05×10^{-5}

[a] Optical band gap (E_g) obtained from the normalized PL and absorption spectra. [b] HOMO level is calculated from $E_{HOMO} = -5.11-(E^{ox}_{1/2}$ vs. Fc/Fc^+), where $E^{ox}_{1/2}$ vs. Fc/Fc^+ is the average value of the first redox peaks with reference to ferrocene. [c] Calculated from LUMO = HOMO + E_g. [d] *M*: hole mobility.

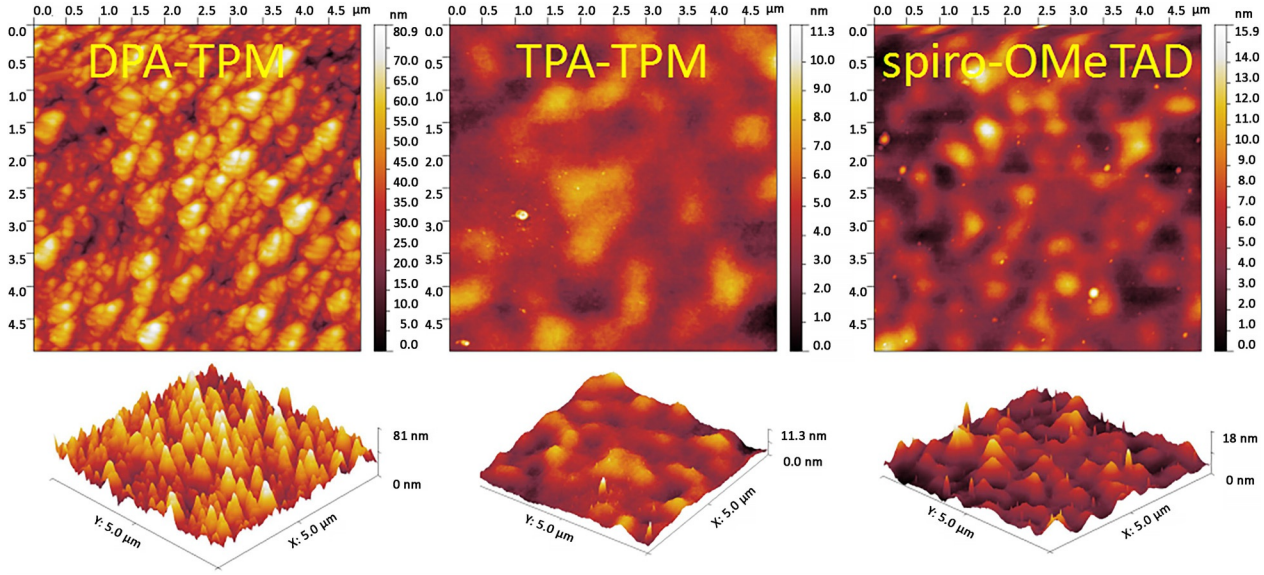

Figure 4. AFM topographical images of HTM films based on DPA-TPM, TPA-TPM, and spiro-OMeTAD.

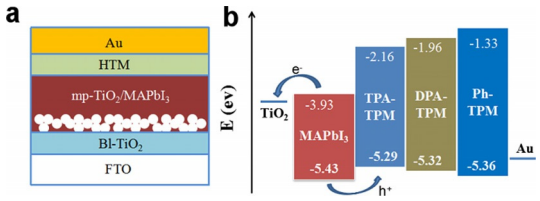

Figure 5. a) Device architecture, and b) energy level diagram of PSCs with two new HTMs.

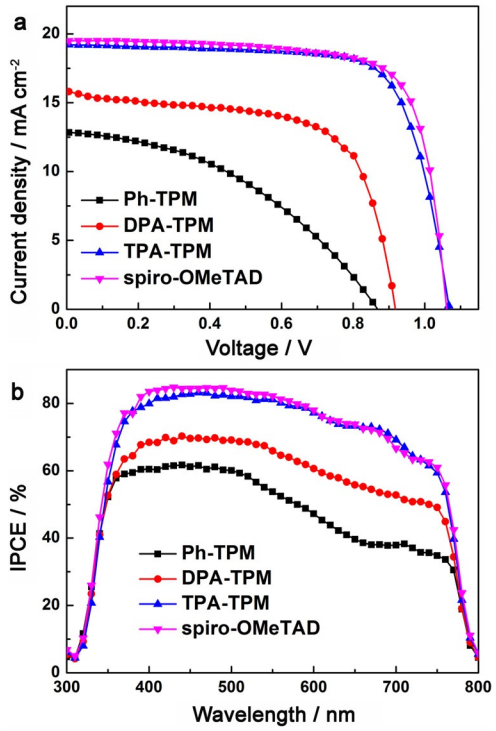

Figure 6. a) *J*–*V* curves, and b) IPCE spectra of the devices with different HTMs.

Table 2. Summary of device parameters with different HTMs.

HTM	V_{oc} [V]	J_{sc} [mA cm^{-2}]	FF [%]	PCE [%]
Ph-TPM	0.87	12.82	42	4.62
DPA-TPM	0.92	15.81	64	9.33
TPA-TPM	1.07	19.19	73	15.06
spiro-OMeTAD	1.06	19.49	75	15.49

current (J_{sc}) of 19.19 mA cm^{-2}, an open-circuit voltage (V_{oc}) of 1.07 V, and a fill factor (FF) of 0.73, leading to a PCE of 15.06%. The devices performance with TPA-TPM are comparable with that of spiro-OMeTAD under the same conditions, with J_{sc} of 19.49 mA cm^{-2}, V_{oc} of 1.06 V, and a FF of 0.75, leading a PCE of 15.49%. Moreover, the average PCE value of TPA-TPM-based devices is 13.90%, (shown in Table S3), which indicates good reproducibility. Hysteresis behavior of the devices with different compounds as HTM were measured through forward and reverse scans, as shown in Figure S3 and Table S5. The devices with TPA-TPM and spiro-OMeTAD show similar hysteresis.

The V_{oc} of the devices based on different HTMs decreases in the order: TPA-TPM > spiro-OMeTAD > DPA-TPM > Ph-TPM, which is not consistent with HOMO energy levels from our CV data. This could be because the V_{oc} of the devices depends on the recombination, splitting of the Fermi levels for photogenerated charges, and the energetics of the devices.[10,38] Moreover, the poor film-forming properties of Ph-TPM and DPA-TPM may lead to inferior charge-extraction capability, as illustrated in time-integrated PL (TIPL) and time-resolved PL (TRPL) measurements. On the other hand, the J_{sc} of the PSCs with different HTMs decreases in the order: spiro-OMeTAD > TPA-TPM > DPA-TPM > Ph-TPM, which may be attributed to their different hole mobilities.

The incident photo-to-current conversion efficiency (IPCE) spectra of the devices were recorded to further confirm photocurrent density, as shown in Figure 6b. All devices show a re-

marked plateau between 400 and 750 nm owed to the similar fabrication process of the PSCs. In good agreement with those of measured photocurrent density under AM 1.5 G illuminations, the TPA-TPM-based devices enhanced the photocurrent by 400–750 nm relative to that of DPA-TPM by improving charge collection and hole mobility. More efficient charge transfer between the HTMs and perovskite layer indicates easier regeneration, resulting in higher IPCE values.

As the stability is very important for solar cells, we performed aging tests of the $CH_3NH_3PbI_3$-based devices on TPA-TPM and spiro-OMeTAD without encapsulation under the same conditions (humidity around 30% relative humidity without illumination). After 9 days of aging, the TPA-TPM-based cell give ~28% reduction (Figure 7), which is less than the spiro-OMeTAD-based cell (41%) owing to better film-forming ability and molecular thermal stability of TPA-TPM. This result shows that the long-term stability of the devices based on TPA-TPM is better than that of spiro-OMeTAD.

To further prove the potential of the application of TPA-TPM in PSCs, we optimized the devices by compositional engineering of perovskite materials ($(FAPbI_3)_{0.85}(MAPbBr_3)_{0.15}$).[39] After optimization, a 17.42% PCE of spiro-OMeTAD-based device was achieved, as shown in Figure 8 and Table 3. TPA-TPM-based devices show a PCE of 16.76%, which is also comparable with spiro-OMeTAD. We believe that through extensive optimization of the device fabrication and perovskite preparation, PCE values of PSCs employing TPA-TPM close to 20% might be attainable.

The charge-transfer dynamics of the $CH_3NH_3PbI_3$ and the bilayer films (HTM/$CH_3NH_3PbI_3$) were investigated by TIPL and TRPL measurements and the perovskite layer (~100 nm) were deposited on the FTO glass surface. The efficient PL quenching and the reduction of the PL lifetime are attributed to charge extraction at the $CH_3NH_3PbI_3$/HTM interface. Figure 9a shows that the bilayer films present dramatic quenching with respect to $CH_3NH_3PbI_3$ (DPA-TPM: 83%, TPA-TPM: 93%, spiro-OMeTAD: 95%). From TRPL spectra (Figure 9b), the estimated decay times are: 10.3 ns for pristine $CH_3NH_3PbI_3$, 3.4 ns for $CH_3NH_3PbI_3$/DPA-TPM, 2.1 ns for $CH_3NH_3PbI_3$/TPA-TPM, and 1.5 ns for $CH_3NH_3PbI_3$/spiro-OMeTAD. TPA-TPM and spiro-OMeTAD reduced the lifetime of holes at the same level. TIPL and TRPL measurements confirm that TPA-TPM has comparable hole-extraction ability compared with spiro-OMeTAD.

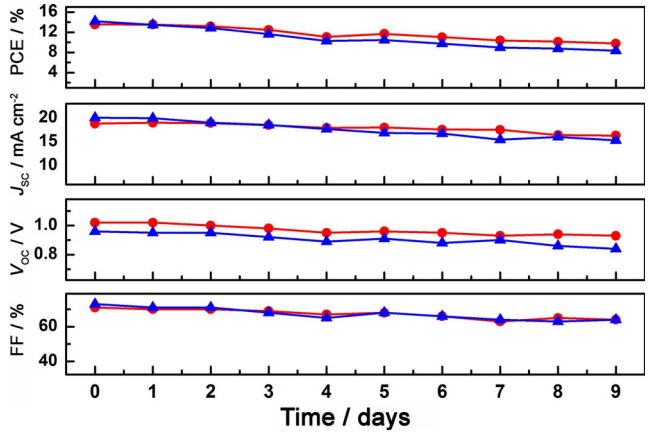

Figure 7. Stability test for $CH_3NH_3PbI_3$-based devices based on TPA-TPM (●) and spiro-OMeTAD (▲) in air at room temperature.

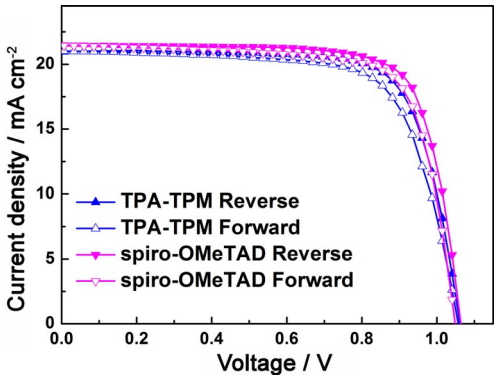

Figure 8. *J–V* curves of the $(FAPbI_3)_{0.85}(MAPbBr_3)_{0.15}$-based devices with TPA-TPM and spiro-OMeTAD.

Table 3. Summary of device parameters with TPA-TPM and spiro-OMeTAD.

HTM	Scan	V_{oc} [V]	J_{sc} [mA cm^{-2}]	FF [%]	PCE [%]
TPA-TPM	reverse	1.06	20.97	75	16.76
	forward	1.06	20.96	71	15.72
spiro-OMeTAD	reverse	1.07	21.44	76	17.42
	forward	1.05	21.43	75	16.76

To further study charge transport and recombination in $CH_3NH_3PbI_3$-based PSCs with different HTMs, impedance spectroscopy (IS) was performed. The recombination resistance (R_{rec}) can be obtained from the high-frequency region of the impedance spectra, where the first arc is related to transport and extraction of cathode/HTM.[40–42] The second arc results from the recombination between TiO_2 and HTMs.[43,44] The devices were analyzed at forward bias between 0.4 and 0.9 V under dark condition. The recombination resistance was fitted using an equivalent circuit model (Figure 10c). As shown in Figure 10a and Figure 10b, the R_{rec} for the devices with TPA-TPM or spiro-OMeTAD show lower values than that of DPA-TPM, which illustrates that the recombination in TPA-TPM or spiro-OMeTAD-based PSCs is lower than that of DPA-TPM-based cells. Therefore, both of PL and IS studies illustrate the devices' better performance with TPA-TPM than with DPA-TPM. Moreover, TPA-TPM with insertion of an extra phenyl group between the nitrogen and TPM show better hole-extraction ability, which results in better device performance.

Conclusions

We developed a series of new hole-transporting materials (HTMs) that incorporated tetraphenylmethane (TPM) as core by a facile synthesis process. Among these developed compounds, TPA-TPM (TPA: arylamine derivates side group) shows good film-forming ability, suitable band alignments with $CH_3NH_3PbI_3$, high thermal stability, and comparable hole mobi-

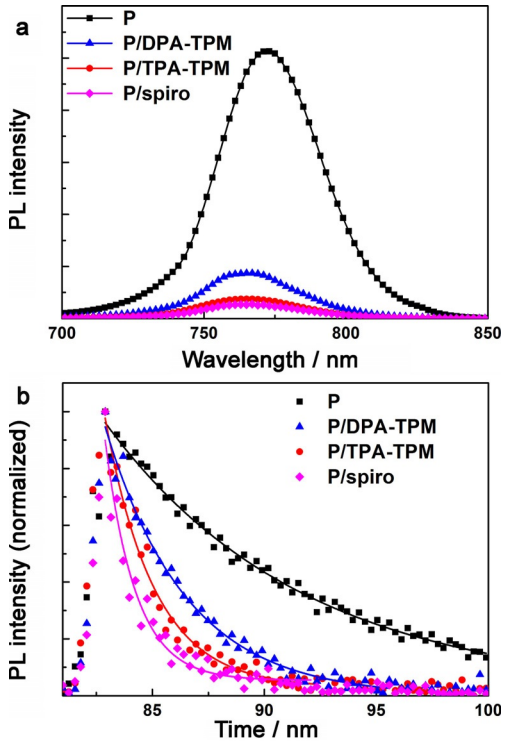

Figure 9. a) TIPL, excitation at 473 nm, and b) TRPL spectra of $CH_3NH_3PbI_3$ (P), P/DPA-TPM, P/TPA-TPM, and P/spiro-OMeTAD. Excitation at 450 nm, monitor at 765 nm.

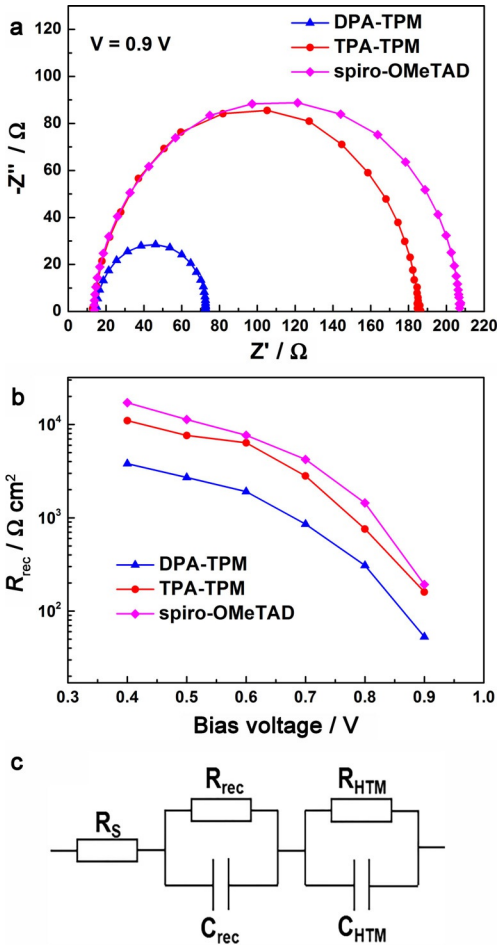

Figure 10. a) Nyquist plots of the device with different HTMs in the dark at 0.9 V bias, b) plots of recombination resistance (R_{rec}) by applying bias voltages, c) equivalent circuit model.

lity to spiro-OMeTAD. Therefore, TPA-TPM shows superior performance when applied in PSCs because of these advantages. The devices fabricated with TPA-TPM show a comparable performance with the current state-of-the-art spiro-OMeTAD. Moreover, the stability of the TPA-TPM-based PSCs is better than that of spiro-OMeTAD. We believe that further modification of the TPM core through molecular engineering of functional groups may further improve the device performance. Our research results also provide a strategy for the design and development of new efficient HTMs for perovskite solar cells.

Experimental Section

Materials

Toluene was dried by 4 Å molecular sieves. 4-methoxy-*N*-(4-methoxyphenyl)-*N*-(4-(4,4,5,5-tetramethyl-1,3,2-dioxaborolan-2-yl)phenyl)aniline (compound **4**) was synthesized and purified in our lab from previous literature.[45,46] Tetrakis(4-bromophenyl)methane, 4,4′-dimethoxydiphenylamine, PbI_2 were purchased from Sigma–Aldrich or TCI. All other chemicals and solvents used in this work were pure grade and used without further purification.

Characterization

^1H NMR and ^{13}C NMR spectra were measured on a Brucker spectrometer (400 MHz). Mass spectra (MS) were performed with a LTQ Orbitrap XL Mass Spectrometer. UV/Vis absorption spectra of the HTMs were obtained on a UV/Vis spectrophotometer (U-3900 H, Hitachi, Japan). TIPL spectra were performed using a standard 450 W xenon CW lamp, and the TRPL were recorded on a pulsed nitrogen/dye laser (QM400, Photo Technology International, USA). CV measurements were performed on a CHI-660d electrochemical analyzer using a standard three-electrode electrochemical cell with a standard calomel reference electrode (SCE), a Pt working electrode and a Pt wire counter electrode. The supporting electrolyte was 0.1 M tetrabutylammonium hexafluorophosphate in CH_2Cl_2, and the scan rate was 50 mV s^{-1}. The monochromatic IPCE spectra were conducted using a QE/IPCE measurement kit (Newport Corporation, USA). DSC of compounds was recorded with scan rate of 20 °C min^{-1} (DSC, TA Instruments-Waters LLC, USA, Q2000).

Synthesis of Ph-TPM, DPA-TPM, and TPA-TPM

The synthesis procedure for Ph-TPM, DPA-TPM, and TPA-TPM is shown in Scheme 1. DPA-TPM and TPA-TPM were synthesized through the Suzuki–Miyaura and Buchwald–Hartwig cross-coupling reactions with high yields, respectively. The detail synthetic procedures are presented as follows.

Ph-TPM. Compound **1** (0.38 g, 0.6 mmol), compound **2** (0.55 g, 3.5 mmol), $Pd(PPh_3)_4$ (58 mg, 0.5 mmol), DMF (20 mL), and 2 M K_2CO_3 (5 mL) were added into a 50 mL flask, then degassed using Ar. The reaction mixture was stirred at 90 °C for 24 h. After cooling down, the reaction mixture was poured into cold Na_2SO_4 aqueous

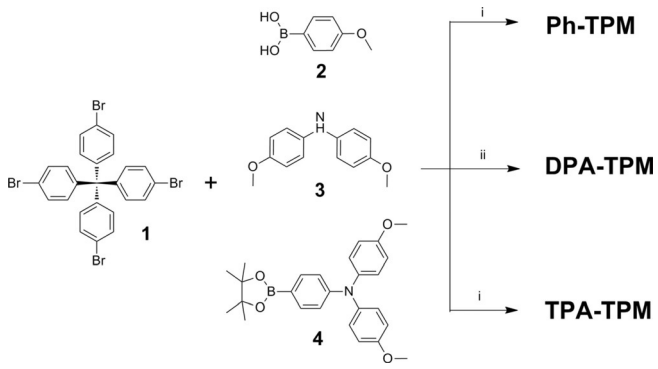

Scheme 1. Synthetic routes for Ph-TPM, DPA-TPM, and TPA-TPM. (i) K_2CO_3, $Pd(PPh_3)_4$, DMF, 90 °C; (ii) *t*BuOK, $Pd(OAc)_2$, $P(tBu)_3$, toluene, reflux.

solution and the crude product precipitates out as solids. The crude product was purified by column chromatography (CH_2Cl_2/PE = 1:1, PE: petroleum ether) to obtain the product as a white solid (0.33 g, 72%). ^{1}H NMR (400 MHz, $CDCl_3$): δ = 7.58 (d, J = 2.9 Hz, 8H); 7.55–7.47 (m, 8H); 7.44–7.35 (m, 8H); 7.00 (d, J = 4.9 Hz, 8H); 3.88 ppm (s, 12H). ^{13}C NMR (100 MHz, $CDCl_3$): δ = 156.05, 148.28, 140.64, 126.71, 126.24, 122.34, 120.52, 114.78, 55.52 ppm. HRMS (MALDI-TOF) *m/z*: [*M*−H] calcd 744.32; found 744.34.

DPA-TPM. Compound **1** (0.64 g, 1 mmol), compound **3** (1.15 g, 5 mmol), *t*BuONa (0.77 g, 8 mmol), $P(tBu)_3$ (0.1 M in toluene, 0.5 mL), $Pd(OAc)_2$ (90 mg, 0.4 mmol) were added into a 50 mL flask and degassed using Ar. Then 20 mL dry toluene was degassed using Ar and injected in to the flask. The reaction mixture was kept with stirring at 100 °C for 2 days. After cooling down, the reaction mixture was diluted by 40 mL CH_2Cl_2 and ished with 80 mL water for 3 times. The organic phase is dried over $NaSO_4$, then removed solvent using a rotary evaporator. The crude product is purified by column chromatography (CH_2Cl_2/PE = 2:1) to obtain the product as white solid (0.92 g, 75%). ^{1}H NMR (400 MHz, $CDCl_3$): δ = 7.06 (d, J = 4.4 Hz, 16H); 6.99 (d, J = 3.3 Hz, 8H); 6.83 (d, J = 4.6 Hz, 24H); 3.81 ppm (s, 24H). ^{13}C NMR (100 MHz, $CDCl_3$): δ = 156.16, 148.53, 140.54, 126.83, 126.55, 126.31, 120.40, 114.82, 55.52 ppm. HRMS (MALDI-TOF) *m/z*: [*M*−H] calcd 1228.46; found 1228.44.

TPA-TPM. Compound **1** (0.51 g, 0.8 mmol), compound **4** (1.72 g, 4 mmol), $Pd(PPh_3)_4$ (70 mg, 0.6 mmol), DMF (20 mL), and 2 M K_2CO_3 (5 mL) were added into a 50 mL flask, then degassed using Ar. The reaction mixture was stirred at 90 °C for 2 days. After cooling down, the reaction mixture was poured into cold Na_2SO_4 aqueous solution, and the crude product precipitate out as solids. The crude product was purified by column chromatography (CH_2Cl_2:PE = 3:2) to obtain the product as a white solid (0.88 g, 72%). ^{1}H NMR (400 MHz, DMSO): δ = 7.55 (d, J = 5.7 Hz, 8H); 7.48 (d, J = 5.9 Hz, 8H); 7.26 (d, J = 7.0 Hz, 8H); 7.05 (d, J = 5.6 Hz, 16H); 6.92 (d, J = 7.4 Hz, 16H); 6.80 (d, J = 6.0 Hz, 8H); 3.74 ppm (s, 24H). ^{13}C NMR (100 MHz, $CDCl_3$): δ = 155.87, 148.07 145.21, 140.98, 138.15, 132.56, 131.52, 127.36, 126.56, 125.41, 120.86, 114.73, 55.51 ppm. HRMS (MALDI-TOF) *m/z*: [*M*−H] calcd 1532.84; found 1532.57.

Device fabrication

F-doped SnO_2 glass substrates were cleaned by sonicating in detergent with surface active agent for 15 min, followed by rinsing with deionized water, and ethanol. Then, a TiO_2 compact layer was deposited on the substrate by spray-pyrolysis deposition method using dry air as carrier gas from a precursor solution of titaniumdiisopropoxide bis(acetylacetonate) in isopropanol solution at 450 °C. The substrates were then annealed at 450 °C for 40 min and cooled down to room temperature. The mesoporous TiO_2 layers were deposited by spin coating at 4000 rpm for 20 s using 30 nm TiO_2 (Dyesol's 30 NR-D Transparent Titania Paste) paste diluted in isopropanol (1:5 weight ratio). The TiO_2 films were sintered at 510 °C for 1 h. After cooling down to 120 °C, the substrates were immediately transferred to a dry air atmosphere. The $CH_3NH_3PbI_3$ films were deposited from a precursor solution containing 1.15 M PbI_2 and 1.10 MAI (Methylamine Hydroiodide) in DMF/DMSO (v:v = 1.5:8.5). The precursor solution was spin coated on the substrates by a two-step program at 1000 rpm for 10 s and 4000 rpm for 30 s. During the second step, 150 μL chlorobenzene was dripped on the substrates at 15 s after starting. The substrates were immediately put in a hot plate and annealed for 1 h. After the substrates were cooled down to RT, the HTM solution (Ph-TPM: 10 mg in 1 mL chlorobenzene, DPA-TPM: 20 mg in 1 mL chlorobenzene, TPA-TPM and spiro-OMeTAD: 60 mg in 1 mL chlorobenzene) containing LiTFSI salt and 4-*tert*-butyl pyridine were deposited by spin coating at 4000 rpm for 30 s. Finally, 60 nm gold electrode was deposited by thermal evaporation under high vacuum.

Acknowledgements

This work was supported by the National Basic Research Program of China (No. 2015CB932200), CAS-Iranian Vice Presidency for Science and Technology Joint Research Project, 116134KYSB20160130, and Natural Science Foundation of Anhui Province (No.1508085SMF224). We acknowledge the Steady High Magnetic Field Facility in High Magnetic Field Laboratory, Chinese Academy of Sciences for the NMR measurements.

Keywords: arylamine · hole-transporting materials · perovskite solar cell · power conversion efficiency · tetraphenylmethane

[1] A. Kojima, K. Teshima, Y. Shirai, T. Miyasaka, *J. Am. Chem. Soc.* **2009**, *131*, 6050–6051.
[2] S. D. Stranks, G. E. Eperon, G. Grancini, C. Menelaou, M. J. Alcocer, T. Leijtens, L. M. Herz, A. Petrozza, H. J. Snaith, *Science* **2013**, *342*, 341–344.
[3] T. Salim, S. Sun, Y. Abe, A. Krishna, A. C. Grimsdale, Y. M. Lam, *J. Mater. Chem. A* **2015**, *3*, 8943–8969.
[4] G. Xing, N. Mathews, S. Sun, S. S. Lim, Y. M. Lam, M. Grätzel, S. Mhaisalkar, T. C. Sum, *Science* **2013**, *342*, 344–347.
[5] W. S. Yang, J. H. Noh, N. J. Jeon, Y. C. Kim, S. Ryu, J. Seo, S. I. Seok, *Science* **2015**, *348*, 1234–1237.
[6] M. A. Green, K. Emery, Y. Hishikawa, W. Warta, E. D. Dunlop, *Prog. Photovoltaics* **2016**, *24*, 905–913.
[7] H.-S. Kim, C.-R. Lee, J.-H. Im, K.-B. Lee, T. Moehl, A. Marchioro, S.-J. Moon, R. Humphry-Baker, J.-H. Yum, J. E. Moser, *Sci. Rep.* **2012**, *2*, 591.
[8] S. Ameen, M. A. Rub, S. A. Kosa, K. A. Alamry, M. S. Akhtar, H.-S. Shin, H.-K. Seo, A. M. Asiri, M. K. Nazeeruddin, *ChemSusChem* **2016**, *9*, 10–27.
[9] P. Gratia, A. Magomedov, T. Malinauskas, M. Daskeviciene, A. Abate, S. Ahmad, M. Grätzel, V. Getautis, M. K. Nazeeruddin, *Angew. Chem. Int. Ed.* **2015**, *54*, 11409–11413; *Angew. Chem.* **2015**, *127*, 11571–11575.
[10] A. Krishna, D. Sabba, H. Li, J. Yin, P. P. Boix, C. Soci, S. G. Mhaisalkar, A. C. Grimsdale, *Chem. Sci.* **2014**, *5*, 2702–2709.
[11] H. Li, K. Fu, P. P. Boix, L. H. Wong, A. Hagfeldt, M. Grätzel, S. G. Mhaisalkar, A. C. Grimsdale, *ChemSusChem* **2014**, *7*, 3420–3425.
[12] T. Malinauskas, M. Saliba, T. Matsui, M. Daskeviciene, S. Urnikaite, P. Gratia, R. Send, H. Wonneberger, I. Bruder, M. Grätzel, *Energy Environ. Sci.* **2016**, *9*, 1681–1686.

[13] H. Choi, S. Paek, N. Lim, Y. H. Lee, M. K. Nazeeruddin, J. Ko, *Chem. Eur. J.* **2014**, *20*, 10894 – 10899.
[14] Y. D. Lin, B. Y. Ke, K. M. Lee, S. H. Chang, K. H. Wang, S. H. Huang, C. G. Wu, P. T. Chou, S. Jhulki, J. N. Moorthy, *ChemSusChem* **2016**, *9*, 274 – 279.
[15] H. Chen, D. Bryant, J. Troughton, M. Kirkus, M. Neophytou, X. Miao, J. R. Durrant, I. McCulloch, *Chem. Mater.* **2016**, *28*, 2515 – 2518.
[16] K. Do, H. Choi, K. Lim, H. Jo, J. W. Cho, M. K. Nazeeruddin, J. Ko, *Chem. Commun.* **2014**, *50*, 10971 – 10974.
[17] K. Rakstys, M. Saliba, P. Gao, P. Gratia, E. Kamarauskas, S. Paek, V. Jankauskas, M. K. Nazeeruddin, *Angew. Chem. Int. Ed.* **2016**, *55*, 7464 – 7468; *Angew. Chem.* **2016**, *128*, 7590 – 7594.
[18] S. Park, J. H. Heo, J. H. Yun, T. S. Jung, K. Kwak, M. J. Ko, C.-H. Cheon, J. Y. Kim, S. H. Im, H. J. Son, *Chem. Sci.* **2016**, *7*, 5517 – 5522.
[19] I. Petrikyte, I. Zimmermann, K. Rakstys, M. Daskeviciene, T. Malinauskas, V. Jankauskas, V. Getautis, M. K. Nazeeruddin, *Nanoscale* **2016**, *8*, 8530 – 8535.
[20] H. Choi, K. Do, S. Park, J. S. Yu, J. Ko, *Chem. Eur. J.* **2015**, *21*, 15919 – 15923.
[21] A. Molina-Ontoria, I. Zimmermann, I. Garcia-Benito, P. Gratia, C. Roldán-Carmona, S. Aghazada, M. Grätzel, M. K. Nazeeruddin, N. Martín, *Angew. Chem. Int. Ed.* **2016**, *55*, 6270 – 6274; *Angew. Chem.* **2016**, *128*, 6378 – 6382.
[22] H. Nishimura, N. Ishida, A. Shimazaki, A. Wakamiya, A. Saeki, L. T. Scott, Y. Murata, *J. Am. Chem. Soc.* **2015**, *137*, 15656 – 15659.
[23] K. Rakstys, A. Abate, M. I. Dar, P. Gao, V. Jankauskas, G. Jacopin, E. Kamarauskas, S. Kazim, S. Ahmad, M. Grätzel, *J. Am. Chem. Soc.* **2015**, *137*, 16172 – 16178.
[24] C. Huang, W. Fu, C.-Z. Li, Z. Zhang, W. Qiu, M. Shi, P. Heremans, A. K.-Y. Jen, H. Chen, *J. Am. Chem. Soc.* **2016**, *138*, 2528 – 2531.
[25] M. Franckevičius, A. Mishra, F. Kreuzer, J. Luo, S. M. Zakeeruddin, M. Grätzel, *Mater. Horiz.* **2015**, *2*, 613 – 618.
[26] P. Ganesan, K. Fu, P. Gao, I. Raabe, K. Schenk, R. Scopelliti, J. Luo, L. H. Wong, M. Grätzel, M. K. Nazeeruddin, *Energy Environ. Sci.* **2015**, *8*, 1986 – 1991.
[27] B. Xu, D. Bi, Y. Hua, P. Liu, M. Cheng, M. Grätzel, L. Kloo, A. Hagfeldt, L. Sun, *Energy Environ. Sci.* **2016**, *9*, 873 – 877.
[28] Y. K. Wang, Z. C. Yuan, G. Z. Shi, Y. X. Li, Q. Li, F. Hui, B. Q. Sun, Z. Q. Jiang, L. S. Liao, *Adv. Funct. Mater.* **2016**, *26*, 1375 – 1381.
[29] S. S. Reddy, K. Gunasekar, J. H. Heo, S. H. Im, C. S. Kim, D.-H. Kim, J. H. Moon, J. Y. Lee, M. Song, S.-H. Jin, *Adv. Mater.* **2016**, *28*, 686 – 693.
[30] H. Lin, S. Chen, H. Hu, L. Zhang, T. Ma, J. Y. L. Lai, Z. Li, A. Qin, X. Huang, B. Tang, H. Yan, *Adv. Mater.* **2016**, *28*, 8546 – 8551.
[31] H.-C. Yeh, R.-H. Lee, L.-H. Chan, T.-Y. J. Lin, C.-T. Chen, E. Balasubramaniam, Y.-T. Tao, *Chem. Mater.* **2001**, *13*, 2788 – 2796.
[32] J.-H. Fournier, X. Wang, J. D. Wuest, *Can. J. Chem.* **2003**, *81*, 376 – 380.
[33] S. Sengupta, S. K. Sadhukhan, S. Muhuri, *Tetrahedron Lett.* **2002**, *43*, 3521 – 3524.
[34] O. Enoki, H. Katoh, K. Yamamoto, *Org. Lett.* **2006**, *8*, 569 – 571.
[35] H. Li, K. Fu, A. Hagfeldt, M. Grätzel, S. G. Mhaisalkar, A. C. Grimsdale, *Angew. Chem. Int. Ed.* **2014**, *53*, 4085 – 4088; *Angew. Chem.* **2014**, *126*, 4169 – 4172.
[36] T. Malinauskas, D. Tomkute-Luksiene, R.d. Sens, M. Daskeviciene, R. Send, H. Wonneberger, V. Jankauskas, I. Bruder, V. Getautis, *ACS Appl. Mater. Interfaces* **2015**, *7*, 11107 – 11116.
[37] J. Burschka, A. Dualeh, F. Kessler, E. Baranoff, N.-L. Cevey-Ha, C. Yi, M. K. Nazeeruddin, M. Grätzel, *J. Am. Chem. Soc.* **2011**, *133*, 18042 – 18045.
[38] N. J. Jeon, J. Lee, J. H. Noh, M. K. Nazeeruddin, M. Grätzel, S. I. Seok, *J. Am. Chem. Soc.* **2013**, *135*, 19087 – 19090.
[39] N. J. Jeon, J. H. Noh, W. S. Yang, Y. C. Kim, S. Ryu, J, Seo, S. I. Seok, *Nature* **2015**, *517*, 476 – 480.
[40] L.-P. Heiniger, F. Giordano, T. Moehl, M. Grätzel, *Adv. Energy Mater.* **2014**, *4*, 1400168.
[41] A. Dualeh, T. Moehl, N. Tetreault, J. Teuscher, P. Gao, M. K. Nazeeruddin, M. Grätzel, *ACS Nano* **2014**, *8*, 362 – 373.
[42] L. Etgar, P. Gao, P. Qin, M. Grätzel, M. K. Nazeeruddin, *J. Mater. Chem. A* **2014**, *2*, 11586 – 11590.
[43] J. A. Christians, R. C. Fung, P. V. Kamat, *J. Am. Chem. Soc.* **2014**, *136*, 758 – 764.
[44] H.-S. Kim, I. Mora-Sero, V. Gonzalez-Pedro, F. Fabregat-Santiago, E. J. Juarez-Perez, N.-G. Park, J. Bisquert, *Nat. Commun.* **2013**, *4*, 2242.
[45] X. Liu, F. Kong, Z. Tan, T. Cheng, W. Chen, T. Yu, F. Guo, J. Chen, J. Yao, S. Dai, *RSC Adv.* **2016**, *6*, 87454 – 87460.
[46] C. Teng, X. Yang, C. Yang, S. Li, M. Cheng, A. Hagfeldt, L. Sun, *J. Phys. Chem. C* **2010**, *114*, 9101 – 9110.

Manuscript received: November 20, 2016
Accepted Article published: December 15, 2016
Final Article published: February 10, 2017